IEEE Access
Multidisciplinary | Rapid Review | Open Access Journal

Received 4 December 2022, accepted 29 December 2022, date of publication 3 January 2023, date of current version 6 January 2023.

Digital Object Identifier 10.1109/ACCESS.2022.3233942

RESEARCH ARTICLE

NOMA-Based Random Access in mMTC XL-MIMO

THIAGO AUGUSTO BRUZA ALVES AND TAUFIK ABRÃO, (Senior Member, IEEE)
Department of Electrical Engineering, State University of Londrina (UEL), Londrina 86057-970, Brazil

Corresponding author: Thiago Augusto Bruza Alves (thiagobruza@hotmail.com)

This work was supported in part by the Coordenação de Aperfeiçoamento de Pessoal de Nível Superior (CAPES) under Grant 001, and in part by the National Council for Scientific and Technological Development (CNPq) of Brazil under Grant 310681/2019-7.

ABSTRACT In machine-type communication (MTC), massive access attempts are generated and the massive MIMO is the key technology to support this demand. To support massive MTC (mMTC), the recent extra-large scale massive multiple-input multiple-output (XL-MIMO) architecture has been seen as a promising technology for providing very high-data rates in high-user density scenarios. Therefore, the large dimension is of the same order as the distances to the user equipment (UE) causing spatial non-stationarities and visibility regions (VRs) to occur across the huge XL array extension. In this work, we investigate the random access (RA) problem in crowded mMTC XL-MIMO scenarios; the proposed grant-based random access (GB-RA) protocol combining the advantage of non-orthogonal multiple access (NOMA) and the strongest user collision resolution in extra-large arrays (SUCRe-XL), namely NOVR-XL scheme can allow access of multiple colliding users in the same XL subarray (SA) selecting the same pilot sequence. The proposed NOVR-XL GB-RA protocol is able to provide a reduction in the number of attempts to access the network, while improving the average sum-rate, as the number of SA increases.

INDEX TERMS NOMA, machine type communication, XL-MIMO, random access protocols, crowded scenarios, uniform rectangular array (URA).

I. INTRODUCTION

There are a large number of users/devices in massive machine-type communications (mMTC) intermittently transmitting modest quantities of data to the base station (BS). This means that the number of active users at any given moment is often substantially lower than the overall number of system users. Simple internet-of-things (IoT) sensors are an example of mMTC devices. Serving those massive connections while guaranteeing a quality of service (QoS) requirement is the prominent challenge in the next generation of multiple access protocols and systems.

The new use case and service classes in 5G systems require significant improvements in physical (PHY) and medium access control (MAC) layers to overcome such challenges. At the PHY layer, the non-orthogonal multiple access (NOMA) transmission schemes is a known and promising candidate for the next generations of multiple access systems, due to its ability to support multiple devices in the same resource element (RE). When compared to the traditional orthogonal multiple access (OMA), the goal consists in attaining higher system throughput and reliability, improving the users' fairness, and reducing latency, while supporting massive connections [1], some types of NOMA schemes with preeminent results are code-domain NOMA, artificial-intelligence NOMA, and power-domain NOMA.

Code-domain NOMA which multiplexing signals in the code-domain was recently explored in [2] to provide connections in overcrowded regime. Artificial-intelligence NOMA in [3] has applied computational learning techniques, such as deep learning in typical NOMA wireless communication systems. Power-domain NOMA is a transmitting structure, proposed initially to improve the spectral efficiency (SE) of wireless networks, sharing the same orthogonal resource, in time and frequency, by combining superposition coding in the transmitter side, and successive interference cancellation (SIC) in the receiver side [4]. In this work we deploy the power-domain NOMA.

A vast number of devices trying to access the network at the same time is a MAC challenge, traditional random

The associate editor coordinating the review of this manuscript and approving it for publication was Walid Al-Hussaibi.

access (RA) schemes are not able to handle such a large number of requests [5], pure RA schemes like ALOHA have severe performance limitation. The incorporation of NOMA significantly improves performance, admitting two users or more per time slot [6].

In massive scenarios, the number of user connections attempting the access the same resource block (RB) far outnumbers the number of available pilot sequences. As a consequence, the implementation of collision resolution protocols becomes essential to allow coherent communication. One well-known decentralized grant-based (RA) protocol for crowded massive multiple-input multiple-output (MIMO) systems is the strongest user collision resolution (SUCRe), which takes advantage of MIMO properties [7], giving preference to the users with good channel conditions, harming edge users.

Seeking to improve RA schemes, the SUCRe protocol [7] has undergone several analyses and improvements. For instance, in [8] a pilot collision reduction strategy was implemented, when compared to [7], making the failed user reselect their pilots by means of an access class barring (ACB) procedure, named idle pilot access (SUCR-IPA) protocol. Another extension is proposed in [9], where a graph-based pilot access (SUCR-GBPA) protocol is proposed, enabling all users who lost contention resolution to choose a new pilot at random. Furthermore, combining NOMA and SUCRe was an important evolution; the work in [10] compares the proposed NOMA-RA protocol to the classical SUCRe scheme, allowing two users trying to access the medium with the same pilot signal to resolve collisions by distinguishing them in the power-domain NOMA and attaining a superior sum-rate performance with reduced average latency.

The recent extra-large scale massive MIMO (XL-MIMO) technology distributes a huge number of antennas elements in a wide space, like facades of buildings, shopping malls, or stadiums; the distance between user equipments (UEs) and the BS antennas might become of the same order of the dimensions of the array [11]. Such arrangement configured special channel conditions, especially unusual channel conditions, such as spatial non-stationarities and *visibility regions* (VRs) [12].

Recently, XL-MIMO systems have received a lot of research interest. Recent papers analyse RA improvements in linear receiver schemes [13], [14], [15], appropriate channel models [12], channel estimation algorithms [16], nonlinear receiver schemes [17], and efficient RA schemes in XL-MIMO [18], [19], [20].

In [13], a revamping in SUCRe protocol enabled its implementation in an XL-MIMO scenarios; the concept of non-overlapping VR was explored in the XL-MIMO context, by associating geographic area and the portion of the array that is visible from that area. Hence, considering that a certain UE is present in that region, the corresponding VR and the associated set of clusters become accessible. Hence, the probability of SA b being visible by UE k can be explored to improve the RA protocol performance in XL-MIMO.

In this work we propose a NOMA grant-based RA protocol for mMTC XL-MIMO scenarios by admitting users colliding, *i.e*, more than one user equipment (UE) selecting the same pilot sequence, and transmitting simultaneously to the same XL subarray, by exploring the advantage of power-domain NOMA.

This work is an extension of our previous work [21]. The *Contribution* of this work is threefold:

- ***i***. we propose a grant-based RA protocol for XL-MIMO systems equipped with power-domain NOMA and by exploring the overlapping VR of XL-MIMO systems (NOVR-XL), combining the advantages of XL-MIMO systems and NOMA, allowing multiple users selecting the same pilot sequence in at least one SA.
- ***ii***. we develop a numerical optimization procedure for the *scale factor* $\delta_{\text{NOVR-XL}}$ in order to maximize the sum-rate of the system; by exploring the NOMA-SIC strategy allows multiple users selecting the same pilot sequence, in a case of possible *false positives*, be resolved converting them into successful attempts, improving the system performance metrics. Besides, aiming to expeditiously maximize the system sum-rate, we propose a look-at-table reference for different loading users and scenarios.
- ***iii***. extensive numerical analyses on the superimposed received signal processed on the SA basis, considering the optimal scale factor $\delta^*_{\text{NOVR-XL}}$ and performing SIC to identify the signal of each user.

The rest of this paper is organized as follows. Section II is described the system model, including the array/subarray integration, while the proposed NOVR-XL is described in Section III. Numerical results are discussed in Section VI. The conclusions are presented in Section V.

A. NOTATIONS

Boldface low-case $\mathbf{a}$ and boldface capital letter $\mathbf{A}$ letters represent, respectively, vectors and matrices. Capital calligraphic letters $\mathcal{A}$ represent finite sets, and $|\mathcal{A}|$ denotes the cardinality. Besides, the operator $\mathcal{A} \subset \mathcal{D}$ denotes the set $\mathcal{A}$ is a subset of $\mathcal{D}$ and $\mathcal{C} = \mathcal{A} \setminus \mathcal{D}$ denotes the set $\mathcal{C}$ is composed by the difference of the set $\mathcal{A}$ and the set $\mathcal{D}$.

The transpose, conjugate-transpose, and conjugate of a matrix $\mathbf{A}$ are denoted by $\mathbf{A}^T$, $\mathbf{A}^H$, and $\mathbf{A}^*$, respectively. We let $\mathbf{I}_M$ denote the $M \times M$ identity matrix, whereas $\|\cdot\|$ stands for the Euclidean norm of a vector. We use $\mathcal{CN}(\mu, \sigma^2)$ to denote circularly-symmetric complex Gaussian distribution with mean μ and variance σ^2, $\mathcal{B}(\cdot,\cdot)$ to denote a binomial distribution, and $\mathbb{C}$ to denote spaces of complex-valued. The Gamma function is denoted by $\Gamma(\cdot)$.

II. SYSTEM MODEL

We consider an XL-MIMO setup where the BS deploys an extra-large antenna array, operating in a time-division-duplexing (TDD). Without loss of generality, we assume a uniform rectangular array (URA) is installed on the y-z plane with a total of M antenna-elements, i.e., $M_y \times M_z$, where

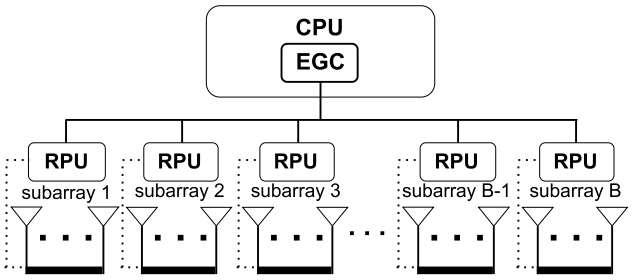

FIGURE 1. Diagram of BS architecture. The antenna array at the BS is composed by *B* SA containing a fixed number of antenna elements M_b. Each SA has an RPU, and all are connected to the EGC in the CPU.

M_y and M_z denote the number of antenna elements along the y-axis and z-axis, respectively, with the firth line of the array starting at the origin O and deployed along the ordinate axis, as in Fig. 3. Similarly, as [13] and [15], we consider a simplified bipartite graph model in XL-MIMO, the array is divided into B subarrays (SAs), each composed by a fixed number of $M_b = M/B$ antennas, ensuring the minimum antennas elements ($M_b \geq 50$), to achieve the inherent properties of massive MIMO [22]. Each SA is equipped with a remote processing unit (RPU) that performs channel estimate, SIC, and resource allocation in a distributed manner, these RPUs are connected to a coordinating central processing unit (CPU), and decoded signals in RPU are sent to CPU to be combined in an equal gain combiner (EGC), where each branch has the same weight, integrated to the BS. All elements are visualized in Fig. 1.

All single-antenna user devices are randomly distributed and grouped in set $\mathcal{U}$, $\mathcal{A} \subset \mathcal{U}$ be the subset of active UEs, with temporarily dedicated data pilots, and $\mathcal{K} = \mathcal{U} \setminus \mathcal{A}$ be the set of inactives UEs (iUEs). The devices in set $\mathcal{K}$ do not have dedicated pilots and if they want to be active, they must be assigned to one. Hence, the number of iUEs in the cell is $|\mathcal{K}| = K$. The BS only allocates pilots to active devices and reclaims the pilots when needed. The iUEs make a RA attempt with probability P_a.

Let $\mathcal{M}$ denote the set of all BS SAs and $\mathcal{V}_k \subset \mathcal{M}$ the subset of SAs visible to the k-th UE. To compose the mathematical modeling, we assume that the subset $\mathcal{V}_k$ is generated at random, where each SA is visible with probability P_b by UE k, like in [13] and [15]. This probability simulates the influence of random obstacles and scatterers in the environment that interact with the signals transmitted by/to the UEs, resulting in VRs. The existence of VRs is evidenced by measurements in [11].

We consider a multiple-user communication systems based on time-frequency coherence blocks and inactive UEs have RA blocks to realize RA attempts. We define τ_{RA} as the number of RA mutually orthogonal pilot sequences that are possible $\mathbf{s}_1, \ldots, s_{\tau_{\text{RA}}} \in \mathbb{C}^{\tau_{\text{RA}} \times 1}$, each with length τ_{RA}, and $\left\| s_{\tau_{\text{RA}}} \right\|^2 = \sqrt{\tau_{\text{RA}}}$.

Since each SA visibility follows a Bernoulli distribution with success probability P_b, it is crucial to note that when

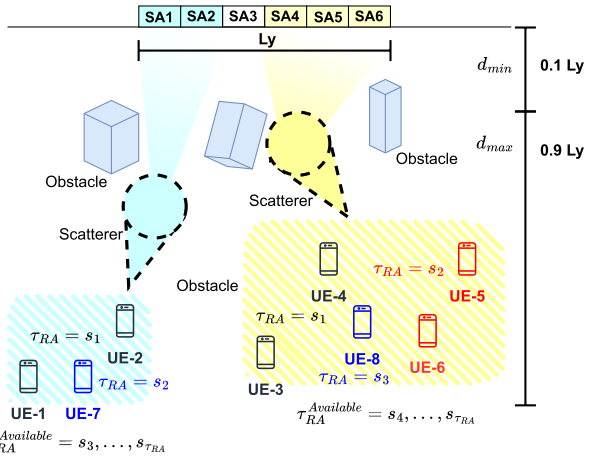

FIGURE 2. Massive MTC system with XL-MIMO URA composed by *B*-SAs containing M_b antennas, the colored regions in each SA define visible UEs, the visibility success probability $P_b = 0.5$ to each SA.

an antenna is visible to a user, it indicates that the user may transmit/receive signals to/from this antenna with a non-zero channel gain [15]. We assume an overcrowded scenario where K iUEs ($K \gg M$) are randomly distributed within a square cell with maximum distance d_{max} and minimum distance d_{min}, respectively, as in Fig. 2.

Due to scatterers and obstacles, whose presence is statistically modeled by the probability of visibility P_b, Fig. 2 illustrates three UEs on the left side having an overlapping VR formed by SA1–SA2: users UE-1 and UE-2 colliding in the same pilot sequence $\mathbf{s}_1$, and UE-7 selects an exclusive pilot sequence $\mathbf{s}_2$, represented by the cyan color area; on the right side, five users having the same VR formed by the SA4–SA5–SA6 identified by the yellow color area; in that SAs, two collisions occur: in the first collision, the UE-3 and UE-4 colliding by sharing the pilot sequence $\mathbf{s}_1$, and UE-5 and UE-6 colliding with pilot sequence $\mathbf{s}_2$; finally, UE-8 selects an exclusive pilot sequence $\mathbf{s}_3$.

In the next step of the proposed protocol NOVR-XL, the orthogonal message of UE-7 is decoded directly at each SA in VR, without interference; besides, the messages of UE-1 and UE-2 collide by sharing the same $\mathbf{s}_1$; hence, such messages can be decoded in SA1 and SA2 by deploying a NOMA scheme, with an application of one SIC step at each SA. In the second SAs group (yellow area), the orthogonal message of UE-8 is decoded directly at each SA in the VR; also, the messages of UE-3 and UE-4 colliding by deploying the same pilot sequence $\mathbf{s}_1$, and the message of UE-5 and UE-6 colliding in the pilot sequence $\mathbf{s}_2$ can be successfully decoded in SA4, SA5, and SA6 by using NOMA, by applying one SIC step. Finally, each decoded signal can be combined in the CPU via EGC combiner. It is important to notice that in the scenario of Fig. 2, SA3 is fully blocked, *i.e.* no UE has SA3 in its VR; hence, such SA3 can be turned off until the channel scenario changes, improving the overall system energy efficiency. Notice that each SA has a dedicated RPU, and the BS has a CPU with EGC and can coordinate the signal processing at each SA.

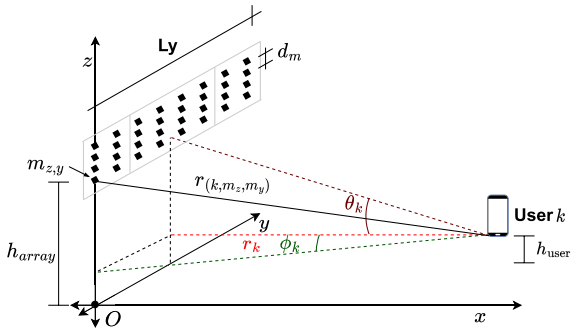

FIGURE 3. Diagram of the kth user at the URA XL-MIMO with an impinging sphere waveform from elevation angle θ and azimuth angle ϕ. The $M = M_y \times M_z$ are horizontally and vertically equally spaced with spacing d_m.

A. CHANNEL MODEL

In the next, we model the NLOS channel based on the position of each URA antenna element $m_{z,y}$, as in Fig 3. The specific localization of $m_{z,y}$-th array element is represented by 3D vector $\mathbf{w}_{m_{z,y}} = [0, (m_y - 1)d_m, h_{array} + (m_z - 1)d_m]$, where $1 \leq m_y \leq M_y$, $1 \leq m_z \leq M_z$, and h_{array} is the height where the array is installed. The physical dimension of the URA along the y-axis and z-axis are $\text{Ly} = (M_y)d_m$ and $\text{Lz} = (M_z)d_m$, where d_m is the distance between elements. The user-k position is defined by 3D vector $\mathbf{q}_k$, the distance of the k-th UE to the specific antenna element $m_{z,y}$ is determined by $r_{k,m_y,m_z} = \left\| w_{m_{z,y}} - q_k \right\|$ [23].

The distance in a straight line perpendicular to the y-axis of the k-th UE of the wide space where the array is installed r_k, and the elevation angle θ_k, formed by r_k and the line between UE_k and the height of array line (red dashed line), and the azimuth angle ϕ_k, formed by the line connecting UE-k to the aperture of $m_{x,y}$ position (green dashed line). Then the location of UE-k is $\mathbf{q}_k = [r_k \Psi_k, r_k \Phi_k, r_k \Omega_k]^{\text{T}}$ with $\Psi_k \triangleq \sin\theta_k \cos\phi_k$, $\Phi_k \triangleq \sin\theta_k \sin\phi_k$ and $\Omega_k \triangleq \cos\theta_k$, $1 \leq k \leq K$. The large-scale fading includes path loss and shadowing, on the basis of an urban micro scenario model provided by [24]:

$$\beta_{k,m_z,m_y} = 10^{-\kappa \log(r_{k,m_z,m_y}) + \frac{g_o + \varphi}{10}}, \tag{1}$$

where $g_o = -34.53$ dB is the path loss at the reference distance, the path loss exponent $\kappa = 3.8$, and $\varphi \sim \mathcal{N}(0, \sigma_{\text{sf}}^2)$ is the shadow fading, a log-normal random variable with standard deviation $\sigma_{\text{sf}} = 10$ dB.

Similarly as [13] and [15], we adopt the average large scale fading for the k-th user at the b-th SA, $\beta_k^{(b)} = \frac{1}{M_b} \sum_{m=1}^{M_b} \beta_{k,m}$. Let $\mathbf{h}_k^{(b)} \in \mathbb{C}^{M_b \times 1}$ be the Rayleigh fading channel vector between UE $k \in \mathcal{K}$ and SA b, following $\mathbf{h}_k^{(b)} \sim \mathcal{CN}\left(0, \beta_k^{(b)} I_{M_b}\right)$.

III. NOVR-XL – RANDOM ACCESS FOR NOMA XL-MIMO

Initially, we explain the four Steps of the SUCRe-XL protocol as depicted in Fig. 4. The operations of the proposed protocol NOVR-XL are detailed in the sequel. Its operations can be seen in Fig. 5. The main difference lies in obtaining and applying at each UE the optimal *scale factor* δ^* which is adjusted aiming to improve the system performance metrics.

A. SUCRe-XL PROTOCOL

The SUCRe-XL protocol [13] is a distributed method for resolving pilot contentions on the user side in XL-MIMO systems. The protocol functionality is illustrated in Fig. 4. Four steps define the SUCRe-XL protocol of [13]:

Step **1**: KP_a users randomly choose an uplink (UL) RA pilot and transmit it;

Step **2**: the BS receives such UE signals and responds with precoded downlink (DL) pilots;

Step **3**: Using the received signal, UEs can estimate the sum of the channel gains of contending UEs for the same RA pilot, comparing the estimate with its own long-term channel gain (estimated in step 0) and retransmitting the chosen RA pilot if it judges it to be the strongest UE among the contenders;

Step **4**: the BS allocates dedicated data pilots to the UEs transmitting in Step before. Users accepted to transmit must fit non-overlapping VRs condition.

After the SUCRe-XL steps, user k in the transmission stage with a dedicated data pilot attains the following SNR in each visible SA-b:

$$\text{SNR}_k^{(b)} = \frac{p_k \beta_k^{(b)}}{\sigma^2}, \tag{2}$$

in which p_k is the user' transmit power.

B. EXPLORING VRs, SubArrays, AND NOMA IN NOVR-XL PROTOCOL

The proposed NOVR-XL protocol deploys the non-overlapping VRs of specific UEs along the SAs aiming to improve the SUCRe-XL protocol [13] operation. Our proposed protocol modifies the *activation decision rule* proposed in the SUCRe-XL protocol [13]. As proposed in [10] we numerically optimize the *scale factor*, namely $\delta_{\text{NOVR-XL}}^{(K,B)^*}$ within the bias parameter ϵ_k, aiming to maximize the system's sum-rate, making more than one user consider themselves able to retransmit the selected pilot (in Step 1); hence, increasing the number of possible *false positives*, *i.e.*, multiple UEs appoint themselves as the contention winner. This is made in a distributed manner, without cooperation with other UEs. Such possible *false positives* can be solved by deploying a NOMA-based scheme, being able to process at the receiver side multiple users sharing the pilot in overlapping VRs, processing on a SA-basis.

Fig. 5 depicts the four steps of the proposed grant-based NOMA XL-MIMO random access protocol and highlights the differences regarding the SUCRe-XL. Also, there is a preliminary Step 0, typically assumed by RA protocols, in which the BS broadcasts a beacon signal; this signal contains enough information to generate time synchronization and send the optimized scale factor $\delta_{\text{NOVR-XL}}^{(K,B)^*}$ values, which is crucial to the well functioning of the proposed NOVR-XL protocol. Indeed, each scenario combining different K-iUEs

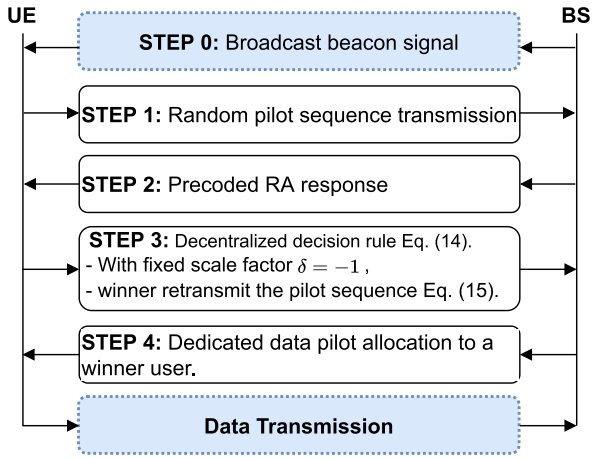

FIGURE 4. Diagram of the steps of the SUCRe-XL random access protocol.

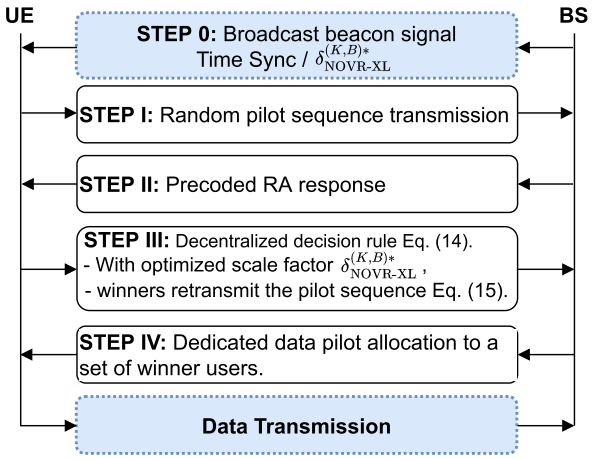

FIGURE 5. Diagram of proposed random access NOVR-XL protocol, the dashed Steps are the same as SUCRe-XL, "STEP 0" and "Data Transmission" phases were included.

and B values requires an optimized *scale factor*, this factor is sent to users in Step 0, and the BS maintains a look-at-table reference with these optimized factors; such a process is explained in Step III. The four steps of the proposed NOVR-XL protocol are described in the following procedure.

Step I: Random Pilot Sequence Transmission: Users in set $\mathcal{K}$ make an RA attempt with a probability P_a, synchronized and δ^* updated by beacon signal in previous Step 0, each UE that wants to be active select uniformly at random one RA pilot sequence $\mathbf{s}_t, t = 1, \ldots, \tau_{\text{RA}}$ and transmits with the user' transmit power p_k. Therefore, let $\mathcal{N}_t \in \mathcal{K}$ be the set of UEs indices that selected pilot t. As in [25], it follows a binomial distribution.

$$|\mathcal{N}_t| \sim \mathcal{B}\left(K, \frac{P_a}{\tau_{\text{RA}}}\right). \tag{3}$$

All inactive UEs that decide to connect transmit RA UL pilot sequences, making SA b receive the signal:

$$Y^{(b)} = \sum_{k\in\mathcal{K}} \sqrt{p_k} h_k^{(b)} s_t^T + N^{(b)}, \tag{4}$$

where $\mathbf{Y}^{(b)} \in \mathbb{C}^{M_b\times\tau_{\text{RA}}}$ and $\mathbf{N}^{(b)} \in \mathbb{C}^{M_b\times\tau_{\text{RA}}}$, with entries drawn from $\mathcal{CN}(0,\sigma^2)$, is the receiver noise. So each SA correlates (4) using an arbitrary normalized pilot $\mathbf{s}_t$, and can estimate the channel of UEs in the same set $\mathcal{N}_t$ yielding:

$$y_t^{(b)} = Y^{(b)}\frac{s_t^*}{\|s_t\|} = \sum_{i\in\mathcal{N}_t}\sqrt{p_i\tau_{\text{RA}}}h_i^{(b)} + n_t, \quad b = 1, \ldots, \text{B}, \tag{5}$$

where $\mathbf{n}_t = N\frac{s_t^*}{\|s_t\|} \sim \mathcal{CN}(0,\sigma^2 I_{M_b})$ is the effective receiver noise. Due the properties of massive MIMO, *channel hardening* and *asymptotic favorable propagation*, we have in each SA:

$$\frac{\left\|\sum_{b\in\mathcal{M}} y_t^{(b)}\right\|^2}{M_b} \xrightarrow{M_b\to\infty} \alpha_t + B\sigma^2, \tag{6}$$

where α_t is the *sum of the signal gains* associated with pilot t in each b-SA:

$$\alpha_t = \sum_{b\in\mathcal{M}}\sum_{i\in\mathcal{N}_t} p_i\beta_i^{(b)}\tau_{\text{RA}}. \tag{7}$$

Step II: Precoded Random Access Response: In SA coordinated mode; SAs transmit a precoded DL pilots to UEs that selected pilot t in Step I.

$$V_{\text{XL}} = \sqrt{\frac{q}{B}}\sum_{t=1}^{\tau_{\text{RA}}}\frac{\sum_{b\in\mathcal{M}} y_t^{(b)*}}{\left\|\sum_{b\in\mathcal{M}} y_t^{(b)}\right\|}s_t^H, \tag{8}$$

where $\mathbf{V}_{\text{XL}} \in \mathbb{C}^{M_b\times\tau_{\text{RA}}}$ and q is the BS transmit power. In this case UEs selecting pilot sequence t receive signal $\mathbf{z}_k^T \in \mathbb{C}^{\tau_{\text{RA}}}$ in the reciprocal channel with receiver noise $\boldsymbol{\eta}_k \sim \mathcal{CN}(0,\sigma^2 I_{\tau_{\text{RA}}})$:

$$z_k^T = \sum_{m\in\mathcal{V}_k} h_k^{(m)T} V_{\text{XL}} + \boldsymbol{\eta}_k^T. \tag{9}$$

From (9), each UE correlates the signal with its RA pilot $\mathbf{s}_t$,

$$z_k = z_k^T\frac{s_t}{\|s_t\|} = \sqrt{\frac{q\tau_{\text{RA}}}{B}}\sum_{m\in\mathcal{V}_k} h_k^{(m)T}\frac{\sum_{b\in\mathcal{M}} y_t^{(b)*}}{\left\|\sum_{b\in\mathcal{M}} y_t^{(b)}\right\|} + \eta_k \tag{10}$$

where $\eta_k = \boldsymbol{\eta}_k\frac{s_t}{\|s_t\|} \sim \mathcal{CN}(0,\sigma^2)$ is the effective receiver noise. To obtain (6) at the UE side, dividing the eq. (10) by $\sqrt{M_b}$ and considering that *asymptotic favorable propagation* and *channel hardening*, it follows that:

$$\frac{z_k}{\sqrt{M_b}} = \sqrt{\frac{q\tau_p}{B}}\frac{\left(\sum_{m\in\mathcal{V}_k} h_k^{(m)T}\sum_{b\in\mathcal{M}} y_t^{(b)}\right)^*}{M_b\sqrt{\frac{1}{M_b}\left\|\sum_{b\in\mathcal{M}} y_t^{(b)}\right\|^2}} + \frac{\eta_k}{\sqrt{M_b}}$$
$$\xrightarrow{M_b\to\infty} \sqrt{\frac{qp_k}{B}}\frac{\sum_{m\in\mathcal{V}_k}\beta_k^{(m)}}{\sqrt{\alpha_t + B\sigma^2}}. \tag{11}$$

Thus, using the function $\Re(\cdot)$ gives the real part of your input and discards the imaginary part, where in this case mitigates noise and estimation errors from eq. (11), resulting:

$$\frac{\Re(z_k)}{\sqrt{M_b}} \approx \tau_{\text{RA}} \sqrt{\frac{qp_k}{B}} \frac{\sum\limits_{m\in\mathcal{V}_k} \beta_k^{(m)}}{\sqrt{\alpha_t + B\sigma^2}} \tag{12}$$

this way each UE-k in $\mathcal{N}_t$ can estimate α_t, so that

$$\hat{\alpha}_{t,k} = \max\left[p_k \sum_{m\in\mathcal{V}_k} \beta_k^{(m)} \tau_{\text{RA}}, \left(\frac{\Gamma(M_b+1/2)}{\Gamma(M_b)}\right)^2 \frac{qp_k\tau_{\text{RA}}^2 \left(\sum_{m\in\mathcal{V}_k} \beta_k^{(m)}\right)^2}{B[\Re(z_k)]^2} - B\sigma^2 \right]. \tag{13}$$

Step III: Contention Resolution with NOMA and Pilot Repetition: By exploring the NOMA, users colliding the same pilot sequence can be served at the same resource, *i.e.*, spatial (SA), frequency, and time.

The collision resolution follows the decentralized decision rule, *i.e.*, each user decides whether to continue in the access attempt, by following the decision rule [10]:

$$p_k \sum_{m\in\mathcal{V}_k} \beta_k^{(m)} \tau_{\text{RA}} > \frac{\hat{\alpha}_{t,k}}{2} + \epsilon_k \tag{14}$$

If inequality in Eq. (14) holds, the user repeats its pilot transmission and forms the new set $\mathcal{S}_t$; otherwise, it remains silent and tries to communicate in the next RA attempt with probability P_{na}. The cardinality of $\mathcal{S}_t$ defines the contention level; indeed, if $|\mathcal{S}_t| = 1$ the collision was solved by the decision rule; otherwise, for $|\mathcal{S}_t| > 1$ (multiple UEs) representing the possible *false positive* case, it will be solved by power-domain NOMA.

$$\mathcal{S}_t = \left\{ k : p_k \sum_{m\in\mathcal{V}_k} \beta_k^{(m)} \tau_{\text{RA}} > \frac{\hat{\alpha}_{t,k}}{2} + \epsilon_k \right\} \tag{15}$$

The decision rule in Eq. (14), presents a bias term ϵ_k, given by:

$$\epsilon_k = \frac{\delta}{\sqrt{M_b} \cdot \sum_{b\in\mathcal{V}_k} \beta_k^{(b)}}, \tag{16}$$

where δ is a *scale factor* that may be adjusted in order to improve the system metrics such as the *average number of access attempts* (ANAA), *fraction of failed access attempts* (FFAA), *normalized number of accepted UEs* (NNAU), *average sum-rate* (aSR), and probability of collision resolution.

Herein, we suggest optimizing the *scale factor* δ numerically, allowing multiple users in the NOVR-XL RA protocol could consider themselves the winners in the contention resolution process, generating *false positive* in SUCRe-XL, which can be resolved in the next step by SIC into the NOMA structure. Indeed, the signal is processed in each SA via RPU by deploying NOMA scheme; hence, resolving overlapping signals via SIC strategy, aiming to decode, reconstruct and cancel the user' signals sharing the same pilot sequence and VR. Finally, the RPU output signals are equally combined in a centralized EGC at the CPU. The purpose of adjustment in the *scale factor* is to attain the system sum-rate maximization. Numerical results section explores the *scale factor* δ optimization.

1) SCALE FACTOR OPTIMIZATION

the optimal value $\delta^{(K,B)^*}_{\text{NOVR-XL}}$ is based on [10], by deploying exhaustive search approach. The procedure is numerically optimal in the sense of sum-rate maximization; hence, each K inactive UEs and B-SA configuration implies an optimal parameter value. To obtain the optimal δ for practical NOMA XL-MIMO system and channel scenarios, the following procedure was adopted:

1) The BS knows the number of SAs B, and an estimation of the number of users intending to become active KP_a[1] present in the cell.
2) Starting with the SUCRe value, $\delta^*_{\text{SUCRe-XL}} = -1$, as in [7], the *scale factor* is tuned iteratively to improve the system sum-rate. Sporadically, motivated by the changes in the physical scenario, BS could re-optimize and broadcast the *scale factor* value in a look-at-table procedure.[2]
3) Select the optimal $\delta^{(K,B)^*}_{\text{NOVR-XL}}$ in the sense that maximizes the system sum-rate, such as:

$$\delta^{(K,B)^*}_{\text{NOVR-XL}} = \underset{\delta}{\text{argmax}}\ R^{\text{NOVR-XL}}_{\sum(K,B)} \tag{17}$$

and record the optimal scale factor in the reference table. Notice that the *scale factor* δ in eq. (16) affects the decision rule defined in Eq. (14), as well as the system sum-rate $R^{\text{NOVR-XL}}_{\sum(K,B)}$ as defined in the sequel, Eq. (22).
4) In a preamble step of the protocol, namely Step 0, taking into account the current system and channel scenario, the BS look-at-table and broadcast the correspondent optimized $\delta^{(K,B)^*}_{\text{NOVR-XL}}$ value.

Without loss of generality, in the contention resolution step the protocol accepts multiple users in NOMA cluster; hence, the BS proceeds with the SIC according to the descending order of channel gains ($\|h_1\| > \|h_k\| > \|h_{|\mathcal{S}_t|}\|$), *i.e.,* the strongest UE-1 signal is decoded first without SIC application, followed by UE-2 signal with one step of SIC to remove UE-1 signal and remaining the interference of UE-3; in the sequel decodes the signal of UE-3 after the two steps SIC of the signal of UE-1 and UE-2, and so on until the last user in set $|\mathcal{S}_t|$.

[1]This estimation process can be obtained by a slight modification of Step 0, by including a tone or pilot sequence transmitted by each user trying to become active.

[2]Look-at-table is a reference table where the BS keeps the optimized values of the scale factor, allowing that each UE could find and use them expeditiously.

The signal-to-interference-plus-noise ratio (SINR) in a SA basis of user k selecting the same pilot sequence t is defined as:

$$\gamma_{t,k}^{(b)} = \frac{p_k \beta_k^{(b)}}{\varpi \sum_{j=1}^{k-1} p_j \beta_j^{(b)} + \sum_{i=k+1}^{|\mathcal{S}_t|} p_i \beta_i^{(b)} + \sigma^2}, \quad (18)$$

where ϖ is the residual interference factor after step SIC assuming imperfect interference cancellation. The rate achieved by each user per SA can be defined as:

$$R_{t,k}^{(b)} = \log_2(1 + \gamma_{t,k}^{(b)}). \quad [bpcu] \quad (19)$$

In our proposed RA protocol, when the distributed *decision rule* results in possible *false positives i.e.*, multiple users repeating the selected pilot after the *decision rule* Eq. (14), these users are grouped in the set $\mathcal{S}_t$ and are treated applying NOMA-SIC strategy, regardless of the cardinality of this set. However, to guarantee that SIC could operate suitably, minimal power differences from colliding UEs' signals must be guaranteed; this can be seen as a minimum SINR among the colliding signals in the same SA. To make a realistic comparison, we adopt a threshold data rate $R_{th}^{(b)}$; hence, users in the set $\mathcal{S}_t$ not satisfying the threshold rate in an SA basis are still deemed *false positives*. Therefore, one can define a new subset of users with successful RA attempt $\mathcal{S}_t^{th}$, formed by collided users achieving the threshold rate as:

$$\mathcal{S}_t^{th} = \left\{ k : R_{t,k}^{(b)} > R_{th}^{(b)} \right\}, \quad (20)$$

which represents those colliding UE' signals resolved by the SIC-NOMA. As a consequence, the subset of *false positive* users $\mathcal{S}_t^{fp}$ hold as:

$$\mathcal{S}_t^{fp} = \mathcal{S}_t \setminus \mathcal{S}_t^{th}. \quad (21)$$

Remark: we named possible *false positive* users in the set $\mathcal{S}_t$, after SIC operation, those users fulfilling the rule Eq. (20), forming the set of users $\mathcal{S}_t^{th}$ that attain successful RA attempt, and a subset $\mathcal{S}_t^{fp}$ named *false positive* users as the subset difference of $\mathcal{S}_t$ and $\mathcal{S}_t^{th}$.

Step IV: The BS estimates the channel[3] to the user, or users, considering the pilot signal sent in Step III, it reconstructs the signal and recurrently applies SIC procedure. After that, the corresponding message is decoded, and users are identified. After decoding is successful a subsequent allocation of the dedicated payload pilots coherence blocks. Unsuccessful UEs are instructed to try again after a random interval, limited to a maximum of 10 attempts, then it stops sending pilot sequence and the packet is considered lost.

In the data transmission step of the SUCRe-XL protocol, only one user is accepted per pilot sequence in non-overlapping VR, on the other hand, in NOVR-XL protocol there will also be multiple users who consider themselves winners in the contention step. The sum-rate of NOVR-XL protocol in an SA basis can be defined using (18) as:

$$R_{\sum(K,B)}^{\text{NOVR-XL}} = \sum_{b\in\mathcal{V}_k} \sum_{t=1}^{\tau_{\text{RA}}} \sum_{k=1}^{|\mathcal{S}_t^{th}|} \log_2\left(1+\gamma_{t,k}^{(b)}\right), \quad [bpcu] \quad (22)$$

While in the SUCRe-XL the sum-rate can be defined as:

$$R_{\sum(K,B)}^{\text{SUCRe-XL}} = \sum_{b\in\mathcal{V}_k} \sum_{t=1}^{\tau_{\text{RA}}} \log_2\left(1+\frac{p_k \beta_k^{(b)}}{\sigma^2}\right), \quad [bpcu] \quad (23)$$

by assuming that just one user per pilot sequence is accepted, and $\delta_{\text{SUCRe-XL}}^{(K,B)^*} = -1$, as in [13].

IV. NUMERICAL RESULTS

It is assumed an URA with $M = 500$ antennas in a $200 \times 100\,\text{m}^2$ cell area with K inactive users (iUEs) randomly distributed as illustrated in Fig. 3, the access probability P_a, the number of available pilots τ_{RA}, and $q = p_k = 1W$. The main simulation parameters are listed in Table 1. The URA has divided in B SA and the visibility success probability $P_b = 0.5$ to each SA. For simulation purposes, $|\mathcal{V}_k| > 0, \ \forall k$, *i.e.,* all users have at least one SA in its VR.

In the numerical simulations, two settings are proposed to evaluate the performance of the NOVR-XL protocol numerically: in setting 1 we assume the SIC running perfectly *i.e.,* $\varpi = 0.00$, and a threshold rate $R_{th_1}^{(b)} = 1.585\,[bpcu]$ is adopted, which represents the signal of interest has a power difference w.r.t. the interference enough to be decoded correctly *i.e.*, $\Delta P \geq 2$. While in setting 2, due fail in any previous crucial process, the SIC is admitted imperfect with residual interference factor $\varpi = 0.10$; this is a typical value of residual factor adopted in NOMA literature [10], [26], and a threshold rate $R_{th_2}^{(b)} = 0.585\,[bpcu]$, hence, the signal of interest can lack enough power difference to be decoded perfectly, in this case, we have adopted $0.5 \leq \Delta P < 2$.

A. SYSTEM SUM-RATE

The optimal value of *scale factor* $\delta_{\text{NOVR-XL}}^{(K,B)^*}$ is obtained numerically based on [10], by exhaustive search approach; it is optimal in the sense of sum-rate maximization; hence, each K-iUE and B-SA configuration requires a search to find the optimal parameter value.

Fig. 6 reveals results for the optimal *scale factor* parameter obtained numerically, following the procedure described in Step III, while it correspondent maximized NOVR-XL sum-rate is shown in Fig. 7, we proposed to consider two different configurations 1 and 2. As evinced, the optimal *scale factor* decreases when the interference increases; whether by the number of UEs contending the pilot grows or when the number of SA decreases.

Notice that the baseline (SUCRe-XL) requires the non-overlapping VR to accept the device; hence, presents a modest gain in terms of sum-rate even increasing the number of SA. The highest sum-rate values occur before the saturation of usage of available pilots. On the other hand, the proposed

[3]For simplicity, and without loss of generality, we consider perfect CSI estimates.

TABLE 1. Simulation parameters.

Parameter	Value
User distance to array	$r_{k,m_z,m_y} \in [10; 180\text{m}]$
User distance from the ground	$h_{user} \in [1; 1.7\text{m}]$
Antennas elements y-axys, z-axys	$M_y = 100, M_z = 5$
Number of BS antennas (URA)	$M = M_y \times M_z = 500$
Number of Subarrays	$B \in \{2; 5; 10\}$
Antenna element distance	$d_m = 1\text{m}$
Array height	$h_{array} = 12\text{m}$
Array length	Ly = $M_y \times d_m$
User transmit power	$p_k = 1\text{W}$
BS transmit power	$q = 1\text{W}$
Noise Power	$\sigma^2 = -98.65\text{dBm}$
Number of iUEs	$K \in [0; 20000]$
Access probability (1^{st} attempt)	$P_a = 0.01$
Access probability (new attempts)	$P_{na} = 0.5$
Number of available pilot sequences	$\tau_{\text{RA}} = 10$
Monte Carlo realizations	5000
Setting 1	
SIC residual	$\varpi = 0.00$
Threshold rate 1	$R_{\text{th}_1}^{(b)} = 1.585$ [bpcu]
Setting 2	
SIC residual	$\varpi = 0.10$
Threshold rate 2	$R_{\text{th}_2}^{(b)} = 0.585$ [bpcu]

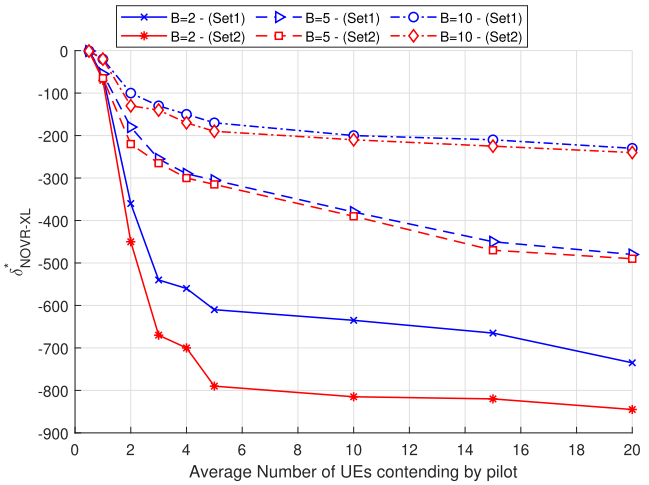

FIGURE 6. $\delta^*_{\text{NOVR-XL}}$ **optimum in terms of sum-rate maximization, obtained numerically for each user loading, both setting 1 and 2, as well for different number of SAs,** $B \in \{2; 5; 10\}$.

NOVR-XL protocol processes the signal superimposed on each SA, canceling the more robust user signal, in some situations, with an assumed residual SIC interference on the order of ϖ, obtaining better sum-rates results when B increases. Also, a higher sum-rate limit is reached when adjusting *scale factor* δ, establishing the maximum number of users selecting the same pilot in the data transmission step; besides, when the number of iUEs grows the *scale factor* value decreases. Notice that the *scale factor* δ value is relatively sensitive to the interference.

In Setting 1, the maximum system sum rate was reached at a loading of $10\,(K \times P_a)/\tau_{RA}$. In Setting 2 the maximum sum-rate was reached at loading $5\,(K \times P_a)/\tau_{RA}$, increasing

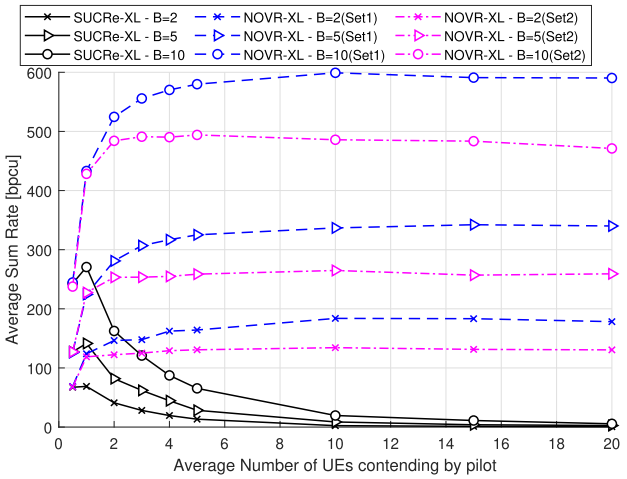

FIGURE 7. Average sum-rate as a function of a number of iUEs. Obtained after adjusting $\delta^*_{\text{NOVR-XL}}$.

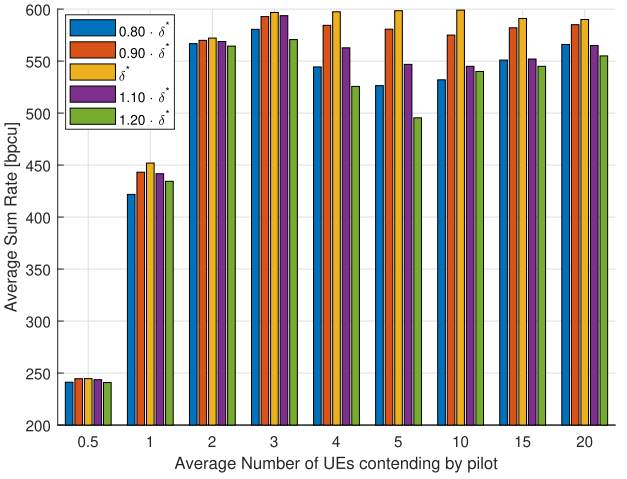

FIGURE 8. Average sum-rate as function of number of iUEs, $B = 10$ **in Setting 1 of NOVR-XL, and sum-rate achieved with** δ **values.**

the load of users from these points observe reduces the sum rate of the system.

In order to verify the sensitivity of the *scale factor* δ^*, Fig. 8 shows the system sum-rate with $B = 10$ SAs. When the interference increases by increasing the number of iUEs K, the sensitivity of the *scale factor* δ on the sum-rate increases substantially, revealing the importance in accurately estimating the *scale factor* parameter in the NOVR-XL protocol context.

B. AVERAGE NUMBER AND FRACTION OF FAILED ACCESS ATTEMPTS

Fig. 9 shows that the proposed protocol NOVR-XL in crowded scenarios ($1 < K \times P_a < 20$) achieves improved RA performance. The modification in decentralized collision resolution is that NOVR-XL accepts multiple users colliding on the overlapping VR, thanks to the power diversity; therefore, the superposition signal can be processed after SIC process

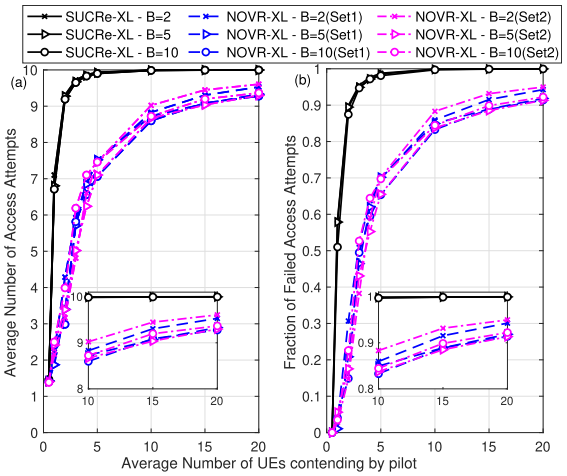

FIGURE 9. RA systems performance. The baseline SUCRe-XL and NOVR-XL. (a) Avg. number of RA attempts. (b) Prob. of failed access attempts.

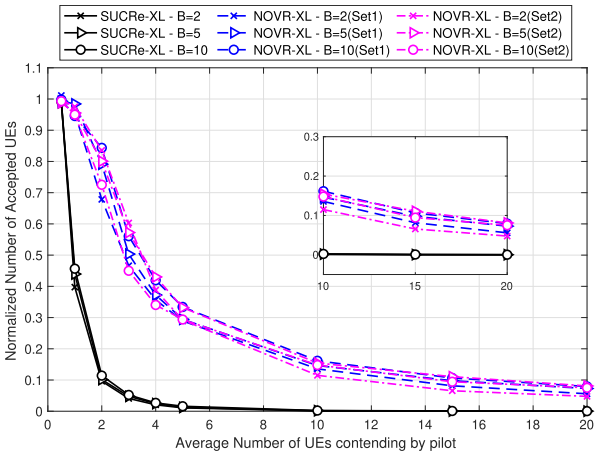

FIGURE 10. Normalized number of accepted UEs, obtained with $\delta^*_{\text{NOVR-XL}}$.

in each SA. With the increase in the number of subarrays B, but constrained by the channel hardening and favorable propagation properties, the probability of collision in each subarray by sharing overlapping VRs in each SA increases. Such collision resolution configuration is impossible to treat with SUCRe-XL due to the absence of the interference cancellation step. As a result, the NOVR-XL allows decreasing the number of access attempts even under solid interference in the same SA.

C. NORMALIZED NUMBER OF ACCEPTED USERS

The normalized number of accepted UEs, calculated by the number of users accepted by the number of users trying to access, given in Fig. 10 corroborate with the improved results in NOVR-XL proposed protocol to accept UEs to transmit due to the superposition signal can be processed by SIC in each SA. In the configuration where the threshold rate is lower setting 2, the residual SIC reduces the users' rate. As the scale factor was optimized to increase the sum rate, high interference reduce the average number of accepted users.

D. COLLISION RESOLUTION

Our approach involves numerically adjusting the *scale factor* to maximize the system's average sum rate, but the two proposed settings have different responses. We consider accepted users who won the contention ($|\mathcal{S}_t| = 1$ and users who are treated by NOMA-SIC ($\mathcal{S}_t^{th}$). In setting 1 the fact that the SIC is perfect the average number of accepted users decreases more slowly and is higher in arrays with more subarrays as shown in Fig. 11 a), the higher threshold rate increase the probability of false positives, in consequence, a higher average sum rate as Fig. 7. On the other hand, in setting 2 there is a residue of interference due to the imperfect SIC which deteriorates the sum rate of NOMA. To maintain the higher level of the sum rate more collisions are resolved without applying NOMA, deteriorating the average number of Accepted UEs, as shown in Fig. 11 b), the lower threshold

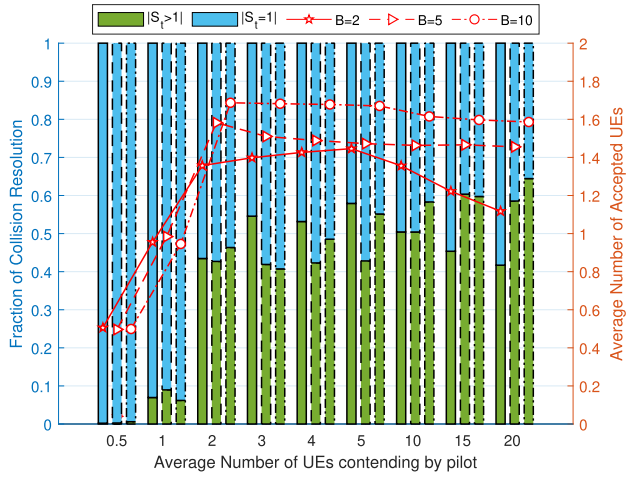

a) Setting 1

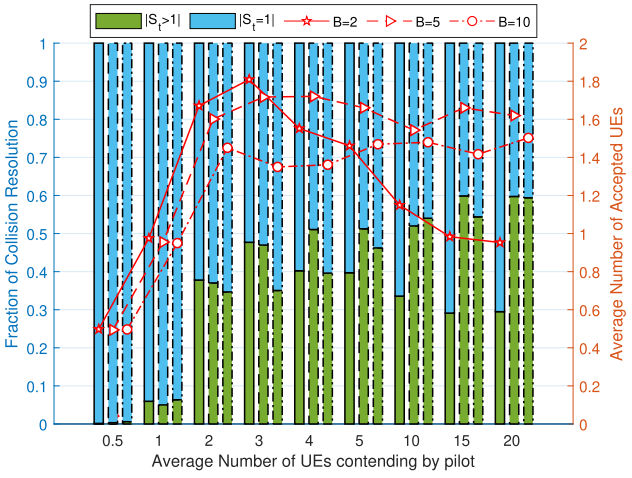

b) Setting 2.

FIGURE 11. Percentage collision resolution by SIC and the average number of Accepted users in NOVR-XL.

rate decrease the probability of false positives in a lower bound in average sum rate as Fig. 7.

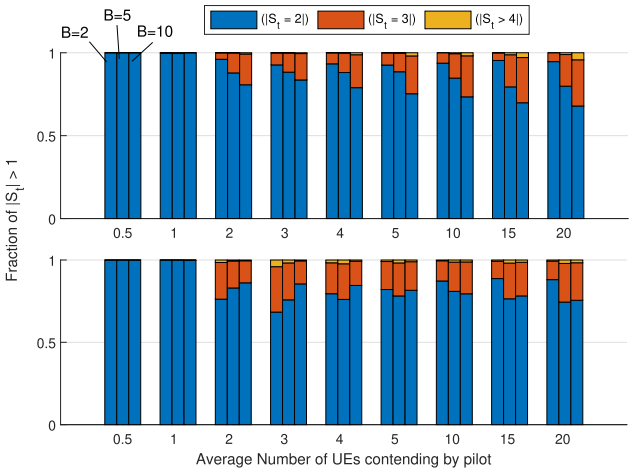

FIGURE 12. Fraction of false positive cases solved by SIC in NOVR-XL. a) Setting 1 and b) Setting 2.

Elaborating further, Fig. 12 analyses the fraction of the number of users in the set $\mathcal{S}_t$ of *false positives* cases resolved by the SIC-NOMA. The figure depicts that the highest number of false positives happens between 2 users, and cases greater than 3 users are rare. The proposed settings substantially change the size of the set $\mathcal{S}_t$ when when changing the number of subarrays B.

E. OVERHEAD, ACCESS TIME DELAY AND COMPLEXITY

The grant-based protocol has a higher overhead because it needs four steps to connect devices to the network. Our proposed protocol NOVR-XL is based on a modification of SUCRe [7], to operate in XL-MIMO [13]. Such a procedure does not cause any overhead or additional time delay compared to the original SUCRe protocol [13]. The numerical optimization and the update of the reference table occur online in system operation and add no overhead to the core of protocol (steps I–IV).

In this application scenario, the proposed protocol improves the access time delay in all studied scenarios, when compared to SUCRe-XL [13], as can be seen in Figure 9.

NOVR-XL complexity that is comparable to SUCRe-XL, the way it is calculated the precoded Random Access Response (8) is the same. The optimized *scale factor* $\delta^{(K,B)*}_{\text{NOVR-XL}}$ eventually shared in Step 0, does not add complexity to the proposed protocol.

V. CONCLUSION

By exploiting power-domain NOMA and signal processing in each SA the grant-based RA protocol performance can be improved. Indeed, the XL-MIMO adds a new degree of freedom with the received signal being processed by different SAs with the support of RPU, together with the degree of freedom introduced by power-domain NOMA, allowing to improve the collision resolution of multiple users using the same pilot sequence in the same VR subarrays, and by applying the SIC stage in each SA at the BS side. Supported by numerical results, we found a substantial performance improvement of the proposed RA protocol regarding the recent literature SUCRe-XL method, with the numerical optimization of *scale factor* δ, in order to maximize the system sum-rate, making multiple users collide deploying the same pilot sequence.

The primary distinction regarding the SUCRe-XL and the NOVR-XL schemes consists of the independent processing per RPU and the collision resolution process. In addition, we unveil the sensitivity of the *scale factor* δ in the NOVR-XL scheme, mainly in scenarios with high interference; hence, the suitable δ value selection is paramount to improve the collision resolution and the system sum-rate. Indeed, in the proposed NOVR-XL protocol, the received superimposed signal data can be properly decoded with SIC steps in a SA basis, even with a rate threshold restriction, and able to achieve both a reduction in the number of access attempts and simultaneously a significant increase in the sum-rate, increasing the average number of accepted users under crowded mMTC scenarios analyzed ($1 < K \times P_a < 20$).

REFERENCES

[1] A. Akbar, S. Jangsher, and F. A. Bhatti, "NOMA and 5G emerging technologies: A survey on issues and solution techniques," *Comput. Netw.*, vol. 190, May 2021, Art. no. 107950.
[2] M. T. P. Le, L. Sanguinetti, E. Bjornson, and M.-G.-D. Benedetto, "Code-domain NOMA in massive MIMO: When is it needed?" *IEEE Trans. Veh. Technol.*, vol. 70, no. 5, pp. 4709–4723, May 2021.
[3] F. Sun, K. Niu, and C. Dong, "Deep learning based joint detection and decoding of non-orthogonal multiple access systems," in *Proc. IEEE Globecom Workshops (GC Wkshps)*, Dec. 2018, pp. 1–5.
[4] O. Maraqa, A. S. Rajasekaran, S. Al-Ahmadi, H. Yanikomeroglu, and S. M. Sait, "A survey of rate-optimal power domain NOMA with enabling technologies of future wireless networks," *IEEE Commun. Surveys Tuts.*, vol. 22, no. 4, pp. 2192–2235, 4th Quart., 2020.
[5] F. Clazzer, A. Munari, G. Liva, F. Lazaro, C. Stefanovic, and P. Popovski, "From 5G to 6G: Has the time for modern random access come?" 2019, *arXiv:1903.03063*.
[6] M. V. da Silva, S. Montejo-Sánchez, R. D. Souza, H. Alves, and T. Abrão, "D2D assisted *Q*-learning random access for noma-based MTC networks," *IEEE Access*, vol. 10, pp. 30694–30706, 2022.
[7] E. Björnson, E. de Carvalho, E. G. Larsson, J. H. Sørensen, and P. Popovski, "A random access protocol for pilot allocation in crowded massive MIMO systems," *IEEE Trans. Wireless Commun.*, vol. 16, no. 4, pp. 2220–2234, Apr. 2017.
[8] H. Han and Y. Li, "A high throughput pilot allocation for M2M communication in crowded massive MIMO systems," *IEEE Trans. Veh. Technol.*, vol. 66, no. 10, pp. 9572–9576, Oct. 2017.
[9] H. Han, Y. Li, and X. Guo, "A graph-based random access protocol for crowded massive MIMO systems," *IEEE Trans. Wireless Commun.*, vol. 16, no. 11, pp. 7348–7361, Nov. 2017.
[10] H. D. Pereira, G. Brante, J. Farhat, R. D. Souza, J. C. M. Filho, and T. Abrao, "On the sum-rate of contention resolution in massive MIMO with NOMA," *IEEE Access*, vol. 9, pp. 24965–24974, 2021.
[11] E. D. Carvalho, A. Ali, A. Amiri, M. Angjelichinoski, and R. W. Heath Jr., "Non-stationarities in extra-large-scale massive MIMO," *IEEE Wireless Commun.*, vol. 27, no. 4, pp. 74–80, Aug. 2020.
[12] J. Flordelis, X. Li, O. Edfors, and F. Tufvesson, "Massive MIMO extensions to the COST 2100 channel model: Modeling and validation," *IEEE Trans. Wireless Commun.*, vol. 19, no. 1, pp. 380–394, Jan. 2020.
[13] O. S. Nishimura, J. C. Marinello, and T. Abrao, "A grant-based random access protocol in extra-large massive MIMO system," *IEEE Commun. Lett.*, vol. 24, no. 11, pp. 2478–2482, Nov. 2020.
[14] O. S. Nishimura, J. C. M. Filho, T. Abrão, and R. D. Souza, "Fairness in a class barring power control random access protocol for crowded XL-MIMO systems," *IEEE Syst. J.*, vol. 16, no. 3, pp. 4574–4582, Sep. 2022.

[15] J. C. M. Filho, G. Brante, R. D. Souza, and T. Abrao, "Exploring the non-overlapping visibility regions in XL-MIMO random access and scheduling," *IEEE Trans. Wireless Commun.*, vol. 21, no. 8, pp. 6597–6610, Aug. 2022.
[16] Y. Han, S. Jin, C.-K. Wen, and X. Ma, "Channel estimation for extremely large-scale massive MIMO systems," *IEEE Wireless Commun. Lett.*, vol. 9, no. 5, pp. 633–637, May 2020.
[17] V. Croisfelt, A. Amiri, T. Abrao, E. de Carvalho, and P. Popovski, "Accelerated randomized methods for receiver design in extra-large scale MIMO arrays," *IEEE Trans. Veh. Technol.*, vol. 70, no. 7, pp. 6788–6799, Jul. 2021.
[18] J. H. I. de Souza, A. Amiri, T. Abrao, E. de Carvalho, and P. Popovski, "Quasi-distributed antenna selection for spectral efficiency maximization in subarray switching XL-MIMO systems," *IEEE Trans. Veh. Technol.*, vol. 70, no. 7, pp. 6713–6725, Jul. 2021.
[19] L. M. Taniguchi, J. H. I. Souza, D. W. M. Guerra, and T. Abrão, "Resource efficiency and pilot decontamination in XL-MIMO double-scattering correlated channels," *Trans. Emerg. Telecommun. Technol.*, vol. 32, no. 12, p. e4365, Dec. 2021.
[20] J. C. Marinello, T. Abrao, A. Amiri, E. de Carvalho, and P. Popovski, "Antenna selection for improving energy efficiency in XL-MIMO systems," *IEEE Trans. Veh. Technol.*, vol. 69, no. 11, pp. 13305–13318, Nov. 2020.
[21] T. A. B. Alves and T. Abrão, "Crowded MTC random access in NOMA XL-MIMO," in *Proc. IEEE SIoT LABCIoT*, Oct. 2022.
[22] E. Björnson, J. Hoydis, and L. Sanguinetti, "Massive MIMO networks: Spectral, energy, and hardware efficiency," *Found. Trends Signal Process.*, vol. 11, nos. 3–4, pp. 154–655, Nov. 2017.
[23] H. Lu and Y. Zeng, "Near-field modeling and performance analysis for multi-user extremely large-scale MIMO communication," *IEEE Commun. Lett.*, vol. 26, no. 2, pp. 277–281, Feb. 2022.
[24] M. Fallgren and B. Timus, *Deliverable D1.1: Scenarios, Requirements and KPIs for 5G Mobile and Wireless System*, document ICT-317669-METIS, 2013.
[25] E. Bjornson, E. de Carvalho, E. G. Larsson, and P. Popovski, "Random access protocol for massive MIMO: Strongest-user collision resolution (SUCR)," in *Proc. IEEE Int. Conf. Commun. (ICC)*, May 2016, pp. 1–6.
[26] X. Wang, R. Chen, Y. Xu, and Q. Meng, "Low-complexity power allocation in NOMA systems with imperfect SIC for maximizing weighted sum-rate," *IEEE Access*, vol. 7, pp. 94238–94253, 2019.

THIAGO AUGUSTO BRUZA ALVES received the B.S. degree in electrical engineering from the Universidade Norte do Paraná (UNOPAR), and the M.Sc. degree in electrical engineering from the Universidade Estadual de Londrina (UEL), Paraná, Brazil, in 2017. He is currently pursuing the joint Ph.D. degree in electrical engineering with UEL and UTFPR Program. His research interests include machine learning and resource allocation applied to telecommunications, extra large massive MIMO, access protocol for mMTC systems, and application of NOMA technologies.

TAUFIK ABRÃO (Senior Member, IEEE) received the B.S., M.Sc., and Ph.D. degrees in electrical engineering from the Polytechnic School, University of São Paulo, São Paulo, Brazil, in 1992, 1996, and 2001, respectively. Since March 1997, he has been with the Communications Group, Department of Electrical Engineering, Londrina State University, Paraná, Brazil, where he is currently an Associate Professor in telecommunications and the Head of the Telecommunications and Signal Processing Laboratory. From July 2018 to October 2018, he was with the Connectivity Section, Aalborg University, as a Guest Researcher. In 2012, he was an Academic Visitor with the Southampton Wireless Research Group, University of Southampton, U.K. He has also served as an Associate Editor for the IEEE Systems Journal, the IEEE Transactions on Vehicular Technology, the *IET Electronics Letters*, the *ETT* journal (Wiley), and the *AEUe* (Elsevier). Previously, he served as an Associate Editor for the IEEE Communications Surveys and Tutorials, from 2013 to 2017, IEEE Access, from 2016 to 2019, and the *IET Signal Processing*, from 2018 to 2020. His research interests include massive and XL-MIMO, RIS-aided communications, URLLC, mMTC, random access protocols, detection and estimation, NOMA systems, cooperative communication, resource allocation, machine learning-aided communications, and optimization techniques for 5G and 6G wireless systems. He is also a Pq-1D CNPq.